Density Functional Studies of the Spin Density Distribution of the P865 Cation Radical in the Reaction Center of *Rb sphaeroides*

Benjamin Robotham and Patrick J. O'Malley*

School of Chemistry, The University of Manchester, Oxford Road, Manchester M13 9PL, U.K.

Received July 25, 2008; Revised Manuscript Received October 27, 2008

ABSTRACT: Density functional calculations are used to calculate the spin density distribution for the P865 dimer cation radical in the *Rb sphaeroides* reaction center. Comparison between calculated and experimental hyperfine couplings is performed where good agreement is found for the four nitrogen and 12^1 proton methyl group hyperfine couplings. Overall, the spin density ratio between the two halves is in agreement with experimental determinations, although the calculations suggest that significant differences in this ratio exists for different regions of the bacteriochlorophyll macrocycles. Calculated spin density asymmetry changes brought about by mutational changes in the immediate amino acid environment agree with experimental interpretations.

Photosynthesis represents the fundamental biological process in which solar energy is converted into chemical energy (*1*). Photosynthetic systems perform this solar capture by first using an antenna system to capture the energy and then funneling it to a so-called reaction center site, which initiates charge separation via rapid electron transfer across a membrane. In the most extensively investigated reaction center of the purple bacterium, *Rb sphaeroides*, initial electron transfer proceeds from the excited singlet state of the primary donor dimeric bacteriochlorophyll *a* molecule (P865) to an acceptor B_A, a monomeric bacteriochlorophyll *a* molecule, in approximately 3 ps. After another 0.9 ps, the electron is transferred to Φ_A, a bacteriopheophytin **a** molecule, resulting in the formation of a cation−anion radical ion pair (*2*).

To obtain a quantitative understanding of these initial electron-transfer mechanisms, one needs to know the spatial and electronic structure of the electron-transfer pigments involved. The well-resolved structures of certain bacterial reaction centers such as *Rps viridis* and *Rb sphaeroides* provide us with the spatial arrangement of the cofactors involved in electron transfer (*3, 4*). The electronic structure of the pigments involved is not easily probed experimentally, however. EPR[1] and ENDOR/TRIPLE resonance methods have been used to map the unpaired spin densities of the free radicals generated during the one-electron-transfer steps (*5*). These methods predominantly use the proton or nitrogen hyperfine interaction terms to probe the unpaired spin density distribution of the free radical involved. These in turn, can be used to indirectly predict the electron density of the frontier orbitals (HOMO/LUMO) involved in the electron-transfer process. Proton hyperfine couplings provide an indirect probe of the electron density of the frontier orbitals, as spin density at the hydrogens arises usually from spin polarization or hyperconjugation with the main electron system situated on the carbon atoms.

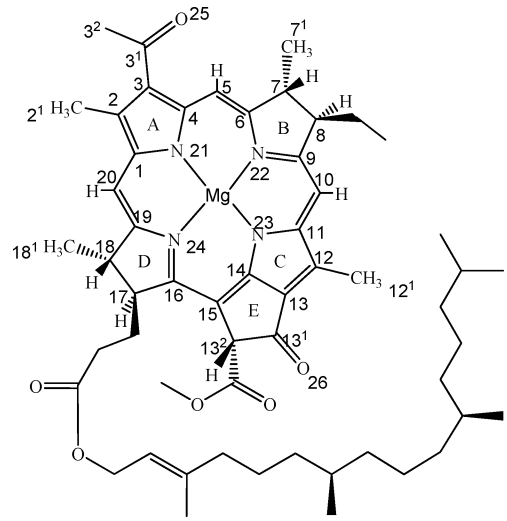

FIGURE 1: Bacteriochlorophyll **a** with standard IUPAC numbering.

Accurate electronic structure prediction methods have been available for some time for small molecular systems. For the size of molecules encountered in photosynthetic electron transfer, more approximate semiempirical methods have been principally employed. With suitable parametrization, the INDO/SP method has been shown to provide good ^{1}H and ^{14}N isotropic hyperfine coupling prediction for chlorophyll molecules in both monomeric and dimeric forms (*6*). Here, s spin populations are calculated, which are then converted to isotropic hyperfine couplings by multiplying by an empirically determined constant for each particular nucleus. As with all such methods, the quality of the results depends on the choice of parameters, and the well-known serious

* To whom correspondence should be addressed. Phone/Fax: 0041612004536. E-mail: patrick.omalley@manchester.ac.uk.

[1] Abbreviations: DFT, density functional theory; B3LYP, Becke3 Lee−Yang−Parr; EPR, electron paramagnetic resonance; ENDOR, electron nuclear double resonance; TRIPLE, electron nuclear nuclear resonance; HOMO, highest occupied molecular orbital; LUMO, lowest unoccupied molecular orbital; INDO/SP, intermediate neglect of differential overlap/spin polarization; ESEEM, electron spin echo envelope modulation.

10.1021/bi801395s CCC: $40.75
Published on Web 11/17/2008

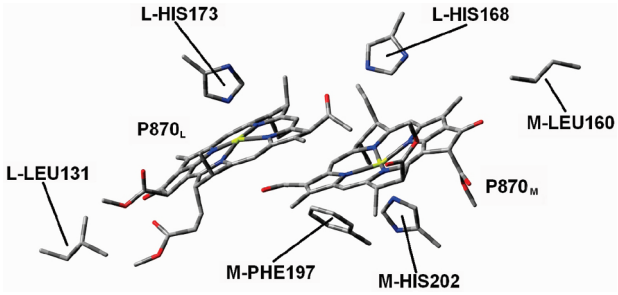

FIGURE 2: The P865 bacteriochlorophyll dimer including amino acid residues from its protein environment: Mg ligating L-His173 and M-His202, L-His168, L-Leu131, M-Leu160, and M-Phe197.

Table 1: Summary of the Dimeric Models Used

cofactors	amino acid residues	notation
P865		P865
P865	L-His173, M-His202	P865_2AA
P865	L-His173, M-His202, L-Leu131, L-His168, M-Leu160, M-Phe197	P865_6AA
P865	L-His173	P865_HET
P865	L-His173, M-His202, L-His168, M-His160	LH(M160)

drawbacks of the INDO method preclude its use as a general method in the study of free radicals. The more recently developed density functional methods, in particular the so-called hybrid methods, now permits highly accurate wave functions to be obtained for large molecular systems. These methods have been particularly impressive in predicting properties of photosynthetic biological free radicals such as semiquinones, chlorophyll, and tyrosyl (*7*−*13*). In contrast to the INDO/SP method described above, isotropic hyperfine couplings are rigorously obtained from a Fermi contact analysis, and anisotropic hyperfine couplings are obtained from the spin only electric field gradient at the nucleus. No empirical parameters are used in the hyperfine coupling calculation. The availability of such exact methods together with the availability of accurate coordinates for the electron-transfer pigments in bacterial photosynthesis permits us to calculate the electronic structure of such pigments and hence provide key insights on electronic pathways for electron transfer.

While the calculated spin density and hyperfine couplings of the monomeric form of the bacteriochlorophyll **a** cation radical (BChl $\mathbf{a}^{+\cdot}$) have been reported (*14, 15*), the same information has not been reported for the dimeric form found in the bacterial reaction center primary donor. Here, we report on the density functional calculated electronic structure of the primary donor for the purple bacterial photosynthetic system, *Rb sphaeroides*, which consists of two symmetrically arranged bacteriochlorophyll **a** molecules labeled $P865_M$ and $P865_L$. The objective of this study is therefore to provide an accurate electronic structure description of the primary donor P865 dimer using density functional theory calculations. The spin density distribution over the two halves of the dimer is investigated using calculated ^{13}C anisotropic hyperfine couplings, and the resultant asymmetry is critically discussed in comparison with asymmetries estimated from experimental hyperfine couplings. To further validate the model, spin density asymmetry introduced by amino acid changes in the vicinity of the dimer are also studied.

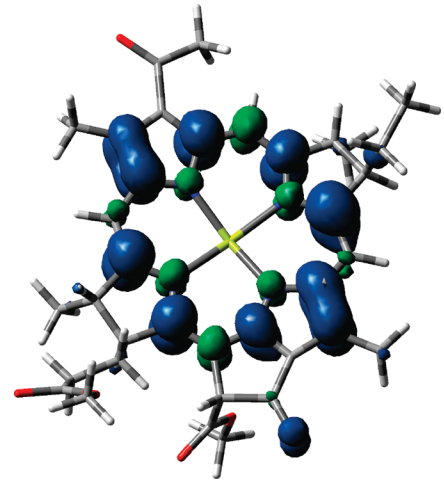

FIGURE 3: Spin density contour (0.002e/au) for the bacteriochlorophyll a monomer model. Blue represents positive spin density and green represents negative spin density. The orientation of the molecule is as given in Figure 1.

MATERIALS AND METHODS

The structure and numbering of the bacteriochlorophyll **a** molecule is shown in Figure 1. The heavy-atom coordinates for P865 and surrounding amino acids used for the calculations were obtained from the crystal-structure of *Rb sphaeroides* as determined by Erlmer et al. (*4*) and obtained from the protein databank (1PCR). All bacteriochlorophyll **a** monomer heavy atom coordinates were taken from the dimer structure and represent one-half of the latter. In all models, the phytyl chain at position 17 was partially truncated to a methyl ester group. Hydrogens were added using standard geometries.

The bare dimer (without any environmental amino acid residues) is our reference structure and is designated P865. In addition, several models incorporating truncated models of amino acids in the immediate dimer environment were included; see Figure 2. The principal amino acid interaction is due to the two Mg ligating histidines L-His173 and M-His290. This model is designated P865_2AA. In addition, models of residues L-His168, M-Phe197, M-Leu160, and L-Leu131 were included in a larger model, P865_6AA. In addition, a model for the heterodimer P865 where the M bacteriochlorophyll **a** half has been replaced by a bacteriopheophytin **a** molecule has been used and is designated P865_HET. In another model, LH(M160), a methylimidazole group has been introduced as a hydrogen bond donor to the 13^1 O atom of the M side. A summary of the models used is given in Table 1. All single point calculations were performed at the UB3LYP/EPR-II for all atoms except Mg where the 6−31G(d) basis set replaced EPR-II. The calculations were performed using Gaussian 03 (*16*).

For monomer calculations, the L and M halves of P865 were used. In addition, a geometry optimized monomer model was prepared both with (BChlMethanol_OPT) and without (BChl_OPT) methanol ligation to the central Mg atom. The geometry of each was fully optimized at the B3LYP/6−31G(d) level of theory.

RESULTS AND DISCUSSION

The monomeric bacteriochlorophyll **a** spin density distribution is shown in Figure 3 demonstrating that positive spin

Table 2: ^{13}C Anisotropic Hyperfine Couplings (T_{11}, T_{22}, T_{33}) for Monomeric Halves of P865_2AA, Dimeric P865_2AA, P865_HET, and LH(M160)[a]

position	L monomer	M monomer	P865_2AA		P865_HET		LH(M160)	
			(L)	(M)	(L)	(M)	(L)	(M)
	−12.5	−11.9	−8.5	−2.8	−10.6	−1.5	−10.1	−1.8
C1	−11.6	−10.9	−7.7	−2.7	−9.7	−1.4	−9.2	−1.8
	24.1	22.8	16.3	5.5	20.3	2.9	19.2	3.6
	−13.3	−12.4	−8.7	−3.2	−11.0	−1.5	−10.4	−2.1
C4	−12.6	−11.7	−8.3	−3.1	−10.4	−1.4	−9.9	−2.1
	25.9	24.1	17.0	6.3	21.4	2.9	20.3	4.2
	−13.7	−13.8	−8.6	−3.9	−11.3	−1.9	−10.2	−2.7
C6	−13.2	−13.4	−8.3	−3.8	−10.9	−1.8	−9.9	−2.7
	26.9	27.2	16.9	7.7	22.2	3.7	20.1	5.4
	−14.6	−14.9	−10.6	−5.7	−12.6	−2.7	−11.3	−4.3
C9	−14.0	−14.3	−10.1	−5.4	−12.1	−2.5	−10.8	−4.1
	28.7	29.2	20.6	11.1	24.7	5.2	22.2	8.5
	−12.0	−12.2	−9.1	−4.8	−10.8	−2.2	−9.6	−3.6
C11	−10.9	−11.1	−8.2	−4.3	−9.9	−1.9	−8.7	−3.2
	22.9	23.3	17.3	9.1	20.7	4.1	18.2	6.8
	−11.2	−11.3	−8.5	−4.3	−9.8	−1.9	−8.9	−3.4
C14	−10.1	−10.3	−7.7	−3.9	−8.9	−1.7	−8.1	−3.1
	21.3	21.6	16.1	8.2	18.8	3.6	17.0	6.4
	−14.9	−13.9	−11.5	−5.4	−12.9	−2.5	−12.0	−4.1
C16	−14.4	−13.4	−11.1	−5.2	−13.4	−2.6	−11.6	−3.9
	29.4	27.3	22.6	10.6	26.3	5.1	23.6	8.0
	−13.7	−14.2	−9.8	−3.6	−11.8	−1.9	−11.0	−2.2
C19	−13.1	−13.6	−9.3	−3.4	−11.3	−1.7	−10.5	−2.1
	26.8	27.7	19.1	6.9	23.1	3.6	21.6	4.3

[a] All values are given in MHz.

density is located at positions C1, C2, C4, C6, C9, C11, C12, C14, C16, and C19 each corresponding to maximum amplitude electron density positions of the singly occupied molecular orbital. Negative spin density is predominantly found at the C5, C10, C15, and C20 positions and also at the four nitrogens. An excellent quantitative measures of the spin density on the ring, which are in principle also experimentally attainable, are the values of the calculated anisotropic hyperfine coupling for the ^{13}C nucleus (*17*). The values for the L and M monomer halves of the P865 dimer are given in Table 2. For large π spin density values around the carbon nucleus, the ^{13}C anisotropic hyperfine couplings give rise to a traceless tensor with the large positive value located along the z axis defined as perpendicular to the ring plane. The values in Table 2 show that the spin density is evenly distributed around the four bacteriochlorin rings concentrated at carbon positions C2, C4, C6, C9, C11, C14, C17, and C19; the values at the C6, C9, C16, and C19 are slightly larger due to the absence of a delocalization pathway for the reduced rings B and D. The spin density distribution for the P865 dimer is shown in Figure 4 at different contour values. The tighter contour shows spin density predominantly on the L half of the dimer. The more diffuse spin density contours show spin density appearing on the M half as well. The spin density profile on both halves is similar to the monomer form. This is quantitatively shown in Table 2 where the ^{13}C anisotropic tensor values for both dimer halves of P865_2AA are given. The ratio of these values L/M is given in Table 3 where there is shown to be significant variation around the bacteriochlorophyll macrocycle. For the wild type model, for example, L/M values vary from 3.0 to 1.9, with the higher L/M values found at positions C1, C4, and C19 where the overlap of the two macrocycles occurs. A similar trend is found for the other two models, P865_HET and LH(M160). The calculations predict therefore that oxidation of the P865 dimer molecule leads to an asymmetric spin density distribution over the two halves with the higher spin density positions corresponding to the L half.

Experimentally, the spin density profile of the both the bacteriochlorophyll **a** monomer and P865 dimer have been investigated using EPR, ENDOR, and ESEEM studies to obtain hyperfine coupling constants for nuclei around the ring, which act as probes of the spin density distribution (*5, 18*). The accessible hyperfine couplings are usually ^{1}H and $^{14/15}$N. Unfortunately, the most direct and best measure of spin density, i.e., the ^{13}C hyperfine couplings, have not been reported. The ^{1}H value for substituent methyl groups, 2^1 and 12^1 or the beta protons, 7, 8, 17, and 18 on saturated rings B and D have been widely used to compare the spin density distribution of the bacteriochlorophyll **a** monomer and the P865 dimer cation radicals. It is somewhat unfortunate that all of these groups, except the 12^1 CH_3 couplings, are very sensitive to small conformational changes of the macrocycles, which are often within the error of crystallographic structure determinations. The $^{14/15}$N values are not subject to such errors and are perhaps the best available experimental monitors of the spin density available but are more difficult than the ^{1}H to obtain experimentally.

With these caveats in mind, in Table 4, we compare calculated hyperfine coupling values with experimental values for both the monomeric forms. For the monomer halves, we must bear in mind that the comparison is with experimental values obtained in alcohol solution, and therefore, we also include a model of bacteriochlorophyll **a** ligated

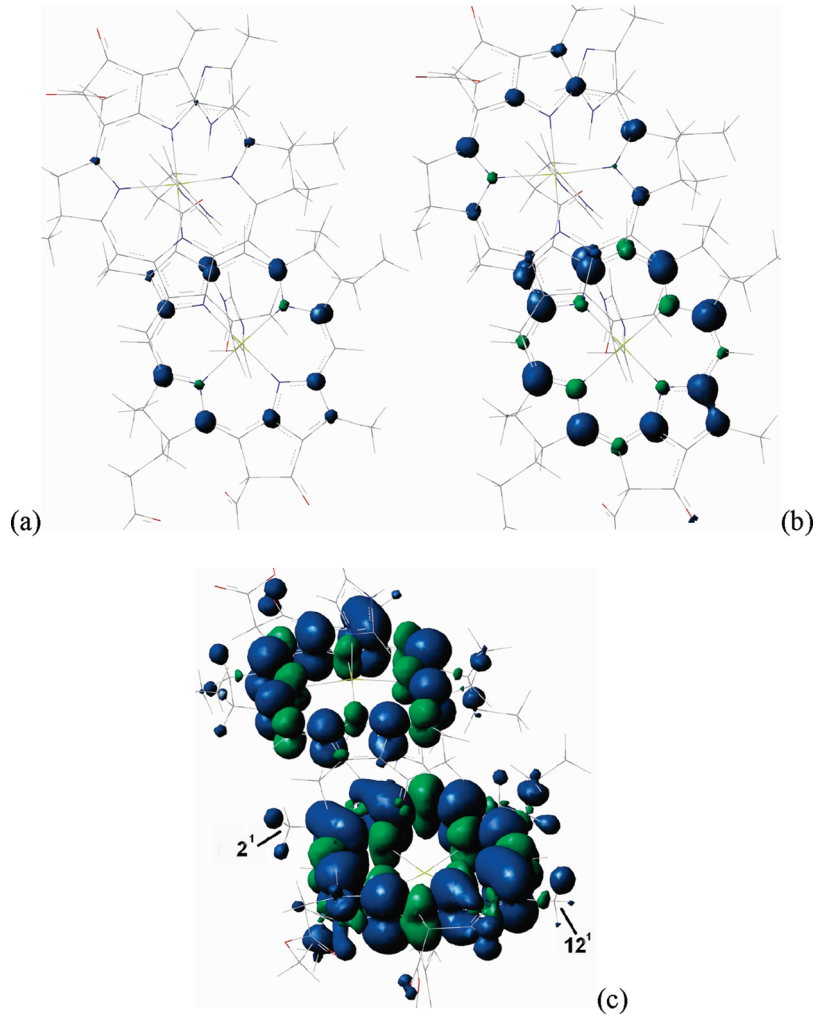

FIGURE 4: Spin density distribution in the P865 radical cation. Spin density contour values shown at (a) 0.008, (b) 0.004, and (c) 0.0004 e/au; blue shows positive, green negative spin density; $P865_L$ is shown below $P865_M$.

Table 3: L/M Ratios Calculated from the Largest Anisotropic ^{13}C Values in Table 1

	P865_2AA	P865_HET	LH(M160)
C1	3.0	7.0	5.3
C4	2.7	7.4	4.8
C6	2.2	6.0	3.7
C9	1.9	4.8	2.6
C11	1.9	5.0	2.7
C14	2.0	5.2	2.7
C16	2.1	5.2	3.0
C19	2.8	6.4	5.0

to a methanol molecule. The values calculated for the nitrogen nuclei are in very good agreement with experimental values and show little variation with the model used demonstrating an invariance to small structure modifications. In general, the 12^1 CH_3 values are in reasonable agreement with the experiment and again are reasonably invariant to the model adapted. For the 2^1 CH_3 couplings, however, the agreement between experimental and calculated values is more mixed. This can be attributed to the sensitivity of these couplings to the orientation of the 3 acetyl group. It can be shown (unpublished data) that the value of the 2^1 CH_3 coupling varies between 4 and 9 MHz depending on the orientation of the 3 acetyl group, which accounts for the variation in values shown in Table 4 for the different models. Because of this uncertainty, we do not consider the 2^1 CH_3 as a reliable assessor of the spin density distribution in the P865 dimer as its value is highly dependent on the 3 acetyl group orientation, which cannot be accurately assessed within the crystal structure resolution. The other values that have been used for comparison experimentally are the protons at positions 7, 8 and 17, 18. These protons receive spin density via hyperconjugation with the large spin density values at positions C6, C9, C16, and C19. As previously emphasized, hyperconjugation will be extremely sensitive to the conformation of the rings B and D. This is clearly shown by the wide variation in the monomer values for the L and M monomer halves of the dimer in Table 4. Due therefore to the limited resolution of the crystal structure determination, use of these values in assessing the spin density distribution of the dimer is likely to be unreliable.

Table 5 compares calculated and experimental hyperfine coupling values for the P865 dimer with and without neighboring amino acid residues. Extending the base dimer model P865 by central Mg ligation, P865_2AA, does lead to small changes in the calculated ^1H and ^{14}N hyperfine couplings reflecting a slight readjustment of the spin density asymmetry between the two halves caused by Mg ligation. Inclusion of further amino acids, P865_6AA, does not lead to any further changes. Comparison of calculated and experimental values in Table 5 shows that the calculated values for the native P865 dimer are in good agreement with

Table 4: Comparison of Experimental to Calculated Isotropic ^1H, ^{14}N Hyperfine Couplings [MHz] for Various Monomeric Models of the Bacteriochloropyll **a** Radical Cation

atom	experimental (*5, 18*)	L-BChl	L-BChl/L-HIS173	BChl_OPT	BChlMethanol_OPT	M-BChl
N21	−2.3	−2.4	−2.3	−2.6	−2.5	−2.7
N22	−3.1	−3.7	−3.6	−3.5	−3.4	−3.5
N23	−2.3	−2.4	−2.2	−2.6	−2.5	−2.4
N24	−2.9	−3.9	−3.8	−3.7	−3.7	−3.7
$H12^1$-av.	9.6	8.7	9.0	10.1	10.1	8.2
$H2^1$-av.	4.9	4.2	4.4	8.6	8.7	6.5
H7	13.5	10.3	7.9	16.6	15.4	5.4
H8	16.4	10.4	10.1	19.9	18.5	6.4
H17	13.1	10.3	10.8	15.9	14.4	23.7
H18	11.8	6.6	8.2	14.6	13.1	21.6

Table 5: Comparison of ^{14}N and ^1H calculated and experimental hyperfine couplings for various P865 models. All values given in MHz.

nucleus	experimental (*21*−*23*)	P865	P865_2AA	P865_6AA	P865_HET	LH(M160)
N21(L) A	−1.7(−1.9)[a]	−1.9	−1.4	−1.6		
N22(L) B	−2.1(−2.5)[a]	−2.6	−2.4	−2.5		
N23(L) C	−1.9(−1.9)[a]	−2.0	−1.7	−1.7		
N24(L) D	−2.3(−2.7)[a]	−3.4	−3.0	−2.9		
N21(M) A	−0.9(−0.4)[a]	−0.4	−0.6	−0.5		
N22(M) B	−0.9(−0.4)[a]	−0.7	−1.1	−1.1		
N23(M) C	−0.9(−0.5)[a]	−0.7	−0.9	−0.9		
N24(M) D	−1.1(−0.5)[a]	−1.2	−1.3	−1.3		
$H12^1$-av.(L)	5.8	7.4	6.8	6.5	7.8(7.4)[b]	6.9(7.0)[c]
$H12^1$-av.(M)	3.2	2.6	3.4	3.5		
$H2^1$-av.(L)	4.0	4.0	4.5	4.4	5.4(5.8)[b]	4.8(5.2)[c]
$H2^1$-av.(M)	1.4	−1.0	−0.3	−0.3		
H7 (L)		7.7	5.0	5.4		
H8 (L)	9.8	10.3	6.6	7.9		
H17(L)	8.8	5.9	8.9	9.2		
H18(L)	6.8	5.8	5.2	4.2		
H7 (M)		2.1	1.8	2.2		
H8 (M)	4.6	6.9	2.8	3.0		
H17(M)		4.51.1	8.8	8.6		
H18(M)			5.5	5.0		

[a] Values in parentheses are for the low temperature determination reference (*19*). [b] Values in parentheses are for the heterodimer determination reference (*21*). [c] Values in parentheses are for the LH(160) determination reference (*21*).

experimental determinations for the 12^1 methyl protons and the four nitrogens. Two sets of couplings have been reported for the nitrogens, which have been interpreted as arising from different spin density ratios on the L and the M halves due to different measurement temperatures (*19*). Our modeling studies cannot, however, readily distinguish such a difference. For the more accurately experimentally determined L half-values, both sets of values give equivalent agreement with the calculated ones.

In addition to the native dimer, mutational studies have succeeded in generating a heterodimer where the M side bacteriochlorophyll **a** has been replaced by a bacteriopheophytin **a** molecule (*20*). Experimentally, the hyperfine couplings have been interpreted to indicate a complete localization of the spin density on the L half. The ^{13}C principal anisotropic hyperfine coupling values for our model of this heterodimer are given also in Table 2 and are in agreement with the majority of spin density localization on the L half-bacteriochlorophyll **a**, although the L/M ratios in Table 3 suggest that some spin density still resides on the M half. Experimentally, the 2^1 and 12^1 methyl group hyperfine couplings have been determined for this heterodimer, and bearing in mind the limitations discussed above, very satisfactory agreement with the values calculated are observed as shown in Table 4. In addition, another mutant LH(M160) (*21*) has been found experimentally to have an increased L/M spin density asymmetry similar to that found for the heterodimer. For our model of this additional hydrogen bonding to the 13^1 O of the M side macrocycle, Tables 2, 3, and 5 show that the calculations do indeed show an increased L/M asymmetry providing a solid validation of our modeling method.

The recent density functional based study of Yamasaki et al. (*12*) reported a somewhat smaller asymmetry compared to that reported here. The study did, however, use a more restricted model than that used here with all nonpolar side groups of the dimer replaced by hydrogen atoms. Methyl and alkyl groups can be expected to have a significant influence on the relative energy of the molecular orbitals of both halves, which may give rise to the differences observed. No hyperfine couplings were reported for comparison with experimental determinations, and the influence of mutational studies on the predicted spin density asymmetry was not reported.

CONCLUSIONS

In conclusion, therefore, DFT calculations on the primary donor P865 cation radical of *Rb sphaeroides* show an asymmetry in the spin density distribution. Comparison of calculated ^1H and ^{14}N hyperfine couplings with experimental determinations shows good agreement for the 12^1 CH_3 group and the four ring nitrogens. The poorer agreement for the 2^1 CH_3 and 7, 8, 17, and 18 protons is attributed to conformational changes, which are not resolved in the crystal structure determination. Calculated spin density asymmetry changes

brought about by mutational changes in the immediate amino acid environment are in agreement with experimental interpretations.

REFERENCES

1. Blankenship, R. E. (2002) *Molecular Mechanisms of Photosynthesis*, Blackwell Science, Oxford, U.K.
2. Feher, G., Allen, J. P., Okamura, M. Y., and Rees, D. C. (1989) Structure and function of bacterial photosynthetic reaction centers. *Nature (London) 339*, 111–116.
3. Deisenhofer, J., and Michel, H. (1989) The photosynthetic reaction center from the purple bacterium *Rhodopseudomonas viridis*. *EMBO J. 8*, 2149–2170.
4. Ermler, U., Fritzsch, G., Buchanan, S. K., and Michel, H. (1994) Structure of the photosynthetic reaction-center from *Rhodobacter sphaeroides* at 2.65-Angstrom resolution: cofactors and protein-cofactor interactions. *Structure 2*, 925–936.
5. Lubitz, W. (1991) In *Chlorophylls* (Scheer, H., Ed.) pp 901−934, CRC Press, Boca Raton, FL.
6. Burghaus, O., Plato, M., Bumann, D., Neumann, B., Lubitz, W., and Mobius, K. (1991) 3 Mm Epr investigation of the primary donor cation radical P865+. in single-crystals of *Rhodobacter sphaeroides* R-26 reaction centers. *Chem. Phys. Lett. 185*, 381–386.
7. O'Malley, P. J. (2000) Hybrid density functional studies of pheophytin anion radicals: Implications for initial electron transfer in photosynthetic reaction centers. *J. Phys. Chem. B 104*, 2176–2182.
8. O'Malley, P. J. (1999) Hybrid density functional studies of a bacteriopheophytin a model and its anion radical form: Geometry, spin densities, and hyperfine couplings. *J. Comput. Chem. 20*, 1292–1298.
9. O'Malley, P. J. (1997) A hybrid density functional study of the p-benzosemiquinone anion radical: the influence of hydrogen bonding on geometry and hyperfine couplings. *J. Phys. Chem. 101*, 6334–6338.
10. O'Malley, P. J. (1996) 1H, 13C and 17O principal hyperfine tensor determination for the p-benzosemiquinone anion radical using hybrid density functional methods. *Chem. Phys. Lett. 262*, 797–800.
11. O'Malley, P. J., and Ellson, D. (1997) 1H, 13C and 17O isotropic and anisotropic hyperfine coupling prediction for the tyrosyl radical using hybrid density functional methods. *Biochim. Biophys. Acta, Bioenerg. 1320*, 65–72.
12. Yamasaki, H., Nakamura, H., and Takano, Y. (2007) Theoretical analysis of the electronic asymmetry of the special pair in the photosynthetic reaction center: effect of structural asymmetry and protein environment. *Chem. Phys. Lett. 447*, 324–329.
13. Takahashi, R., Hasegawa, K., and Noguchi, T. (2008) Effect of charge distribution over a chlorophyll dimer on the redox potential of P680 in photosystein II as studied by density functional theory calculations. *Biochemistry 47*, 6289–6291.
14. Sinnecker, S., Koch, W., and Lubitz, W. (2000) Bacteriochlorophyll a radical cation and anion-calculation of isotropic hyperfine coupling constants by density functional methods. *Phys. Chem. Chem. Phys. 2*, 4772–4778.
15. Sinnecker, S., Koch, W., and Lubitz, W. (2002) Chlorophyll a radical ions: A density functional study. *J. Phys. Chem. B 106*, 5281–5288.
16. Frisch, M. J., Trucks, G. W., Schlegel, H. B., Scuseria, G. E., Robb, M. A., Cheeseman, J. R., Montgomery, J. A., Jr., Vreven, T., Kudin, K. N., Burant, J. C., Millam, J. M., Iyengar, S. S., Tomasi, J., Barone, V., Mennucci, B., Cossi, M., Scalmani, G., Rega, N., Petersson, G. A., Nakatsuji, H., Hada, M., Ehara, M., Toyota, K., Fukuda, R., Hasegawa, J., Ishida, M., Nakajima, T., Honda, Y., Kitao, O., Nakai, H., Klene, M., Li, X., Knox, J. E., Hratchian, H. P., Cross, J. B., Bakken, V., Adamo, C., Jaramillo, J., Gomperts, R., Stratmann, R. E., Yazyev, O., Austin, A. J., Cammi, R., Pomelli, C., Ochterski, J. W., Ayala, P. Y., Morokuma, K., Voth, G. A., Salvador, P., Dannenberg, J. J., Zakrzewski, V. G., Dapprich, S., Daniels, A. D., Strain, M. C., Farkas, O., Malick, D. K., Rabuck, A. D., Raghavachari, K., Foresman, J. B., Ortiz, J. V., Cui, Q., Baboul, A. G., Clifford, S., Cioslowski, J., Stefanov, B. B., Liu, G., Liashenko, A., Piskorz, P., Komaromi, I., Martin, R. L., Fox, D. J., Keith, T., Al-Laham, M. A., Peng, C. Y., Nanayakkara, A., Challacombe, M., Gill, P. M. W., Johnson, B., Chen, W., Wong, M. W., Gonzalez, C., Pople, J. A. (2003) *Gaussian 03, Revision D.01*, Gaussian, Inc., Pittsburgh PA.
17. Gordy, W. (1980) *Theory and Applications of Electron Spin Resonance*, Wiley, New York.
18. Lubitz, W., Lendzian, F., Plato, M., Scheer, H., and Mobius, K. (1997) *Appl. Magn. Reson. 13*, 531–550.
19. Kass, H., Rautter, J., Bonigk, B., Hofer, P., and Lubitz, W. (1995) 2D ESEEM of the ^{15}N-labeled radical cations of bacteriochlorophyll a and of the primary donor in reaction centers of *Rhodobacter sphaeroides*. *J. Phys. Chem. 99*, 436–448.
20. Williams, J. C., Alden, R. G., Murchison, H. A., Peloquin, J. M., Woodbury, N. W., and Allen, J. P. (1992) Effects of mutations near the bacteriochlorophylls in reaction centers from *Rhodobacter sphaeroides*. *Biochemistry 31*, 11029–11037.
21. Rautter, J., Lendzian, F., Schulz, C., Fetsch, A., Kuhn, M., Lin, X., Williams, J. C., Allen, J. P., and Lubitz, W. (1995) Endor studies of the primary donor cation-radical in mutant reaction centers of *Rhodobacter sphaeroides* with altered hydrogen-bond interactions. *Biochemistry 34*, 8130–8143.
22. Lendzian, F., Bonigk, B., Plato, M., Mobius, K., and Lubitz, W. (1992) In *The Photosynthetic Bacterial Reaction Centre II* (Breton, J., Ed.), pp 89−97, Plenum Press, New York.
23. Lendzian, F., Huber, M., Isaacson, R. A., Endeward, B., Plato, M., Bonigk, B., Mobius, K., Lubitz, W., and Feher, G. (1993) The electronic-structure of the primary donor cation-radical in *Rhodobacter sphaeroides* R-26- endor and triple-resonance studies in single-crystals of reaction centers. *Biochim. Biophys. Acta 1183*, 139–160.

BI801395S